Characterization of $CuInS_2$ thin films prepared by one-step electrodeposition

Y. Di Iorio, M. Berruet, W. Schreiner & M. Vázquez

Journal of Applied Electrochemistry

ISSN 0021-891X
Volume 44
Number 12

J Appl Electrochem (2014) 44:1279-1287
DOI 10.1007/s10800-014-0752-5

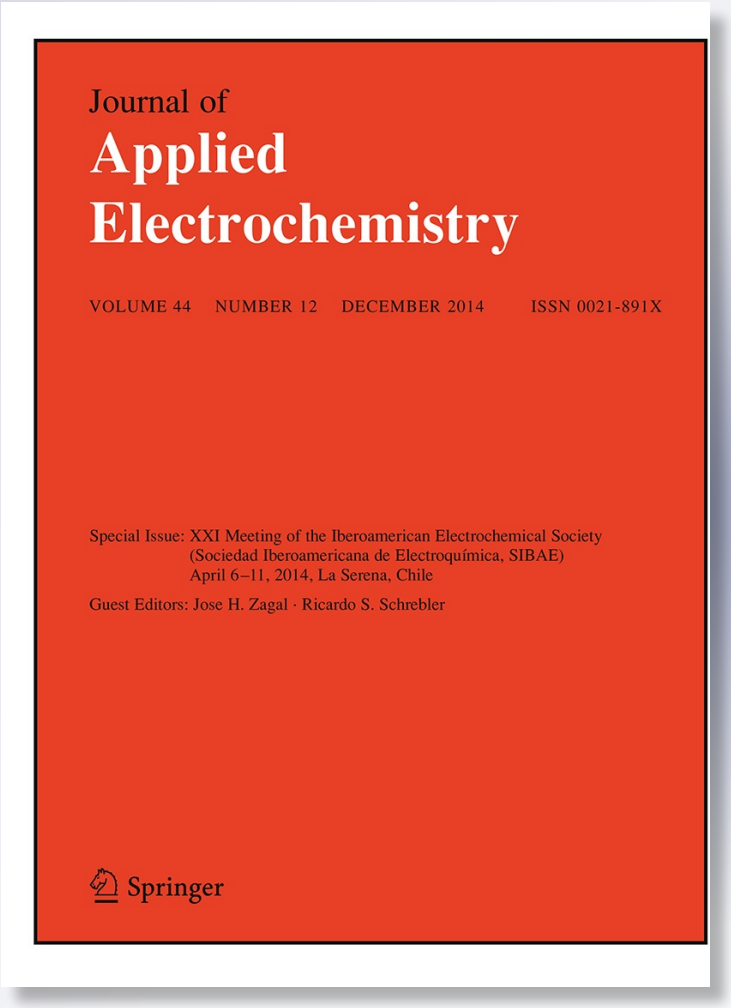

Springer

Your article is protected by copyright and all rights are held exclusively by Springer Science +Business Media Dordrecht. This e-offprint is for personal use only and shall not be self-archived in electronic repositories. If you wish to self-archive your article, please use the accepted manuscript version for posting on your own website. You may further deposit the accepted manuscript version in any repository, provided it is only made publicly available 12 months after official publication or later and provided acknowledgement is given to the original source of publication and a link is inserted to the published article on Springer's website. The link must be accompanied by the following text: "The final publication is available at link.springer.com".

Author's personal copy

J Appl Electrochem (2014) 44:1279–1287
DOI 10.1007/s10800-014-0752-5

RESEARCH ARTICLE

Characterization of $CuInS_2$ thin films prepared by one-step electrodeposition

Y. Di Iorio · M. Berruet · W. Schreiner · M. Vázquez

Received: 29 May 2014 / Accepted: 18 September 2014 / Published online: 1 October 2014
© Springer Science+Business Media Dordrecht 2014

Abstract $CuInS_2$ thin films were fabricated by one-step electrochemical deposition from a single alkaline aqueous solution and using conductive glass as the substrate. The electrolyte consisted in 0.01 mol L^{-1} $CuCl_2$, 0.01 mol L^{-1} $InCl_3$, 0.5 mol L^{-1} Na_2SO_3 and 0.2 mol L^{-1} $Na_3C_3H_5O(COO)_3$ (CitNa) at pH 8. The films were analyzed using a variety of techniques such as X-ray diffractometry, micro-Raman spectroscopy, X-ray energy dispersive spectroscopy, X-ray photoelectron spectroscopy and photoelectrochemistry. After carrying out a thermal treatment in sulfur vapor, chalcopyrite $CuInS_2$ thin films were obtained. Etching the films in KCN solution was found to be a key step, enabling a final adjustment in the stoichiometry. These thin films exhibited *p*-type semiconductor behavior with the bandgap of 1.43 eV. The results show that electrodeposition provides a cost-effective and versatile method for the preparation of thin films of $CuInS_2$, even when acidic precursors need to be avoided.

Keywords Semiconductors · $CuInS_2$ · Electrodeposition · Thin films

Y. Di Iorio · M. Berruet · M. Vázquez (✉)
División Electroquímica y Corrosión, INTEMA, CONICET, Facultad de Ingeniería, Universidad Nacional de Mar del Plata, Juan B. Justo 4302, B7608FDQ Mar del Plata, Argentina
e-mail: mvazquez@fi.mdp.edu.ar

W. Schreiner
Laboratório de Superfícies e Interfases, Departamento de Física, Universidade Federal do Paraná, Curitiba, Paraná 81531-990, Brazil

1 Introduction

$CuInS_2$ is an absorber material suitable to be used in thin film solar cells due to several interesting properties, including a high absorption coefficient (around of 10^5 cm^{-1}) and a band gap value within 1.3–1.5 eV, which is close to the optimum range for photovoltaic conversion. $CuInS_2$ is of particular interest for being environmentally friendly, principally when compared to $CuInSe_2$ where the high toxicity of Se represents a disadvantage.

There are numerous methods to deposit thin films of CIS [1–4], such as spray pyrolysis [5, 6], thermal evaporation [7], chemical bath deposition [8], and electrodeposition [9–11]. Electrodeposition is an attractive method for thin layers production because it is easily scalable, cost-effective and suitable for various types of conductive substrates [1]. However, as it is a ternary compound, the purity, stoichiometry, and physical properties of $CuInS_2$ thin films prepared using one-step electrodeposition can be difficult to control. Few studies have reported detailed physical properties of $CuInS_2$ samples obtained using one-step electrodeposition [1, 3, 11–16]. Furthermore, most of the reported depositions of $CuInS_2$ were carried out in acidic aqueous solutions within a pH range of 1.1–3.4. For example, Sanchez et al. [12] prepared Cu–In–S thin films on glass coated with fluorine-doped tin oxide (FTO) using one-step electrodeposition at pH 3. Yuan et al. [13] electrodeposited Cu–In precursors at pH 4 and annealed the samples in a sulfur atmosphere. To our knowledge, there are no reports of depositions at higher pH values. This represents a drawback when acidic precursors need to be avoided to guarantee the stability of the support material. This is the case of ZnO, its amphoteric nature and the ease with which it dissolves at extreme pH values, can be a problem when used in contact with acidic precursors. This

Author's personal copy

n type semiconductor has been used widely as substrate in the preparation of superstrate cells [2, 12, 17–19]. This study is a preliminary investigation to explore the viability of electrodeposition of CIS on ZnO. For this reason, the first stage is to evaluate the electrodeposition of $CuInS_2$ films on fluorine-doped tin oxide (FTO) coated glass substrates, within the pH window where ZnO is stable.

The electrolyte consisted of aqueous solutions of $CuCl_2$, $InCl_3$, Na_2SO_3 as precursors, and $Na_3C_3H_5O(COO)_3$ (Cit-Na) as chelating agent. This produced a stable and transparent electrolyte without Cu and In compounds precipitating. Cyclic voltammetry was used to study the deposition potentials in the alkaline electrolyte. The crystalline degree, morphology and composition of the annealed films were characterized by X-ray diffraction (XRD), micro-Raman spectroscopy, X-ray photoelectron spectroscopy (XPS) and scanning electron microscopy (SEM) combined with X-ray energy dispersive spectroscopy (EDS). Relevant photoelectrochemical properties of the samples were studied under illumination.

2 Experimental details

2.1 Substrate

Glass coated with a transparent conducting tin oxide (FTO, SnO_2:F, Libbey Owens Ford, TEC 8/3: sheet resistance 8 Ω/sq, thickness 3 mm) was used as substrate. Prior to use, the substrates were degreased with detergent solution and then rinsed in an ultrasonic bath with ethanol and acetone during 10 min respectively. The substrate was cut into square pieces (2×2 cm^2) and the active geometrical area was limited to 1.22 cm^2 by the electrochemical cell design.

2.2 Electrochemical deposition

The electrodeposition of the CIS films was carried out using a standard three-electrode cell; FTO and a saturated calomel electrode (SCE) were used as working and reference electrodes respectively. A Pt mesh of big area was employed as counter electrode. The electrodeposition was carried out at a fixed potential value ($E = -1.2$ V vs. SCE) during 90 min using a Voltalab PGP 201 potentiostat and a stagnant solution at 30 °C.

The precursor solution consisted of 0.01 mol L^{-1} $CuCl_2$ (Sigma-Aldrich, purity > 97 %), 0.01 mol L^{-1} $InCl_3$ (Sigma-Aldrich, purity > 97 %), 0.50 mol L^{-1} Na_2SO_3 (Cicarelli, purity > 99 %) and 0.2 mol L^{-1} $Na_3C_3H_5O(COO)_3$ (Biopack, purity > 99 %). Sodium citrate (Cit-Na) is introduced as complexing agent. The solution was stirred continuously during 1 h. The pH value of the electrolytic bath was adjusted to 8 by appropriated addition of HCl or NaOH from stock solutions.

Once the electrodeposition was completed, an annealing step was undertaken in sulfur vapor atmosphere (sulfur powder at 450 °C) for 90 min using a purpose built reactor. After the thermal treatment, unreacted secondary phases were chemically etched by immersion in 0.5 mol L^{-1} KCN solutions during 30 s [20–23]. This KCN treatment is used to selectively remove copper sulfides from the CIS surface. During the etch, Cu(I) and Cu(II) sulfides dissolve, forming Cu cyanides and Cu cyanocuprates.

2.3 Characterization

Cyclic voltammograms were carried out using a standard three-electrode cell, as described above. The voltammograms of each component and of the electrolytic bath were recorded applying a scan rate of 10 mVs^{-1}.

The films were analyzed by XRD using a PANalytical X'Pert Pro diffractometer, Cu-Kα ($\lambda = 1.541$ Å) radiation at 40 kV and 40 mA. The samples were scanned between 20° and 80° at a speed of 0.02 °/s. The crystallographic data for each phase were taken from the literature and analyzed with X'Pert HighScore software.

Localized Raman spectra were performed using an Invia Reflex confocal Raman microprobe. Excitation was provided with the 514 nm emission line of an Ar^+ laser. The measurements were carried out in backscattering configuration using a 50× objective. Raman micro-mapping was performed scanning a rectangular zone (20×60 μm) in the sample and recording a total of 250 spectra.

The morphology and cross-sections of the layers was studied with SEM, using a JEOL JSM-6460LV microscope. The thickness of the films was evaluated using a KLA TENCOR D-100 profilometer.

The composition was analyzed by X-ray (EDS). The system used is an EDAX Genesis XM4-Sys 60, equipped with Multichannel Analyzer EDAX mod EDAM IV, Sapphire Si(Li) detector and Super Ultra-Thin Window of Be, and EDAX Genesis software.

X-ray photoelectron spectroscopy (XPS) spectra were registered using a commercial VG Microtech ESCA 3000 system. The spectra were collected using Al–K radiation. Survey spectra were recorded for the samples in the 0– 1,100 eV binding energy range by 1 eV steps and a bandpass of 50 eV. High resolution scans with 0.1 eV steps and bandpass of 20 eV were conducted over the following regions of interest: In 3*d*, *S* 2*p*, Cu 2*p*. In every case, surface charging effects were compensated by referencing the binding energy (BE) to the C 1 s line of residual carbon set at 284.5 eV BE [24].

The optical properties of the films, such as transmittance spectra and the direct band gap energy, eg., were recorded

Author's personal copy

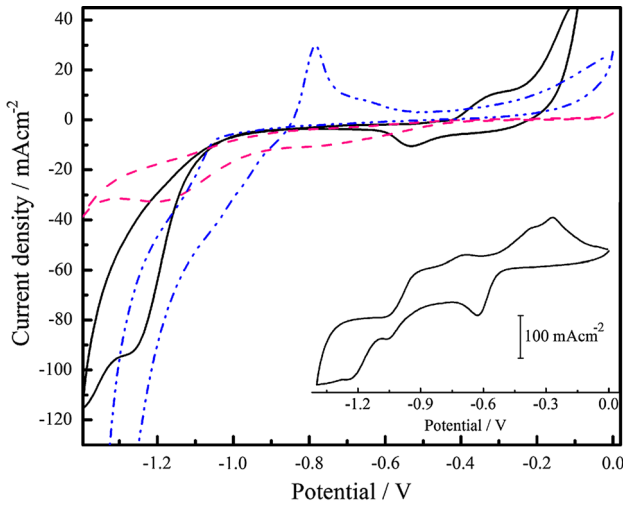

Fig. 1 Cyclic voltammograms of FTO substrates in: (*solid line*) 0.01 mol L^{-1} $CuCl_2$ + 0.2 mol L^{-1} CitNa, (*dashed line*) 0.01 mol L^{-1} $InCl_3$ + 0.2 mol L^{-1} CitNa and (*dash doted ine*) 0.50 mol L^{-1} Na_2SO_3 + 0.2 mol L^{-1} CitNa. *Inset* cyclic voltammogram carried out on FTO substrate in a solution with 0.01 mol L^{-1} $CuCl_2$ + 0.01 mol L^{-1} $InCl_3$ + 0.50 mol L^{-1} Na_2SO_3 + 0.2 mol L^{-1} CitNa. All voltammograms were recorded at pH 8, room temperature and at a scan rate of 10 mV s^{-1}

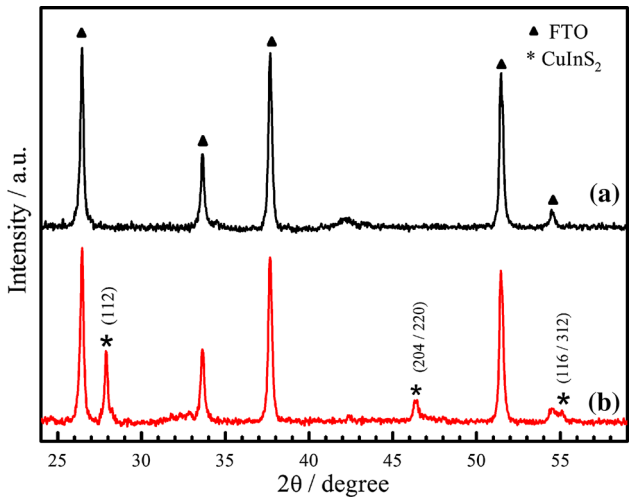

Fig. 2 XRD patterns of CIS thin films deposited at fixed potential (−1.2 V vs SCE) during 90 min at 30° C and at pH 8. **a** As deposited and **b** after annealing in sulfur atmosphere at 450 °C for 90 min

and derived, respectively. The spectra were registered using an UV/Vis spectrophotometer (A 160, Shimadzu) in the wavelength range 350–1,100 nm at room temperature.

Photocurrent and photopotential measurements were performed in the dark and under illumination forming a semiconductor/electrolyte junction by immersion of the FTO/$CuInS_2$ film in 0.1 mol L^{-1} KCl solution. The light source was a 150 W Xe lamp coupled to an air-mass filter 1.5 G (solar simulator, Oriel-Newport 96000). The light beam passes the cell through a quartz window and focuses on the film side of the glass used as substrate. The light was chopped using an electronic shutter (Uniblitz model T132). An IVIUM® compact potentiostat was employed to carry out these measurements.

3 Results and discussion

3.1 Determination of the deposition potential

The electrochemical deposition of the individual components was carried out first, in order to investigate the potential window appropriated to the deposition of each component of the film. The scans started with a negative sweep from an initial potential of 0 V and was scanned at 10 mV s^{-1}. Figure 1 shows the voltammograms recorded on bare FTO electrodes, in three different electrolyte solutions: 0.01 mol L^{-1} $CuCl_2$ with 0.2 mol L^{-1} CitNa, 0.01 mol L^{-1} $InCl_3$ with 0.2 mol L^{-1} CitNa and 0.50 mol L^{-1} Na_2SO_3 with 0.2 mol L^{-1} CitNa. All the solutions were adjusted to pH 8.

The voltammogram obtained using the Cu^{+2} solution shows two reduction peaks, the first cathodic peak at −0.53 V corresponding to the reduction of Cu^{+2} to Cu^{+} and the other at –1.25 V due to the formation of metallic copper. In the case of In^{+3}, one reduction peak can be observed at −1.15 V. The reduction peaks of copper and indium ions appear to be more negative than the reduction potentials without the chelating agent (citrate ions) in the solution. For the curve of sulfite solution with CitNa, the reduction of SO_3^{-2} shows a current peak when the applied potential is close to −1.05 V.

The inset in Fig. 1 shows a cyclic voltammogram carried out using a solution that contains all precursors together at pH 8. The maximum negative current density is registered between −1.2 and −1.3 V. From these results, the potential chosen to perform the electrodeposition of CIS is −1.2 V.

3.2 Characterization of the films

3.2.1 Chemical composition and structural studies

XRD patterns for as-deposited (Fig. 2, curve a) and annealed (Fig. 2, curve b) samples of the electrodeposited thin films are presented. The as-deposited sample is amorphous in nature and does not show any major peak except those corresponding to substrate. As-deposited films present a grayish color that clearly darkens after annealing in the sulfur atmosphere showing good uniformity and adherence. Figure 2, curve b shows that the heat treatment

Author's personal copy

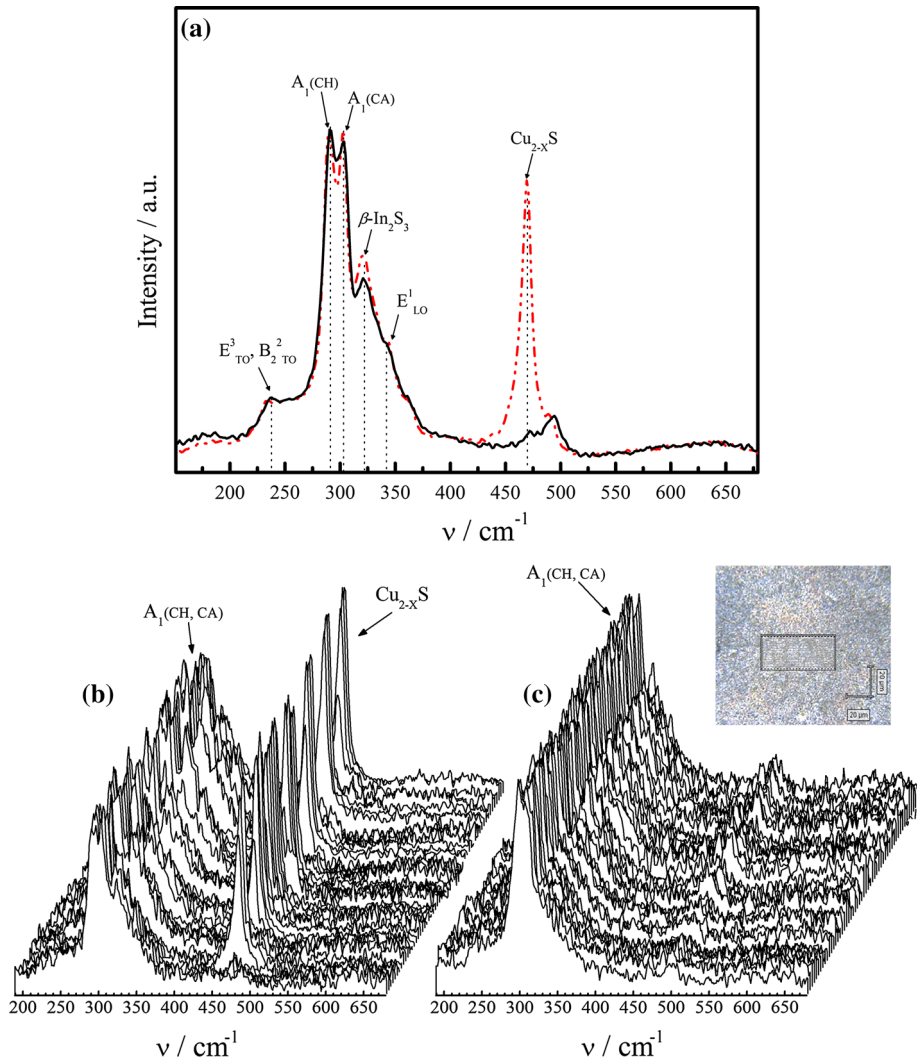

Fig. 3 Raman spectra of CIS films recorded at 514 nm after annealing at 450 °C in sulfur atmosphere for 90 min. **a** Average spectra before (*dashed line*) and after (*solid line*) etching with 0.5 mol L^{-1} of KCN solution during 30 s. **b** and **c** Micro-Raman maps performed over a 20 × 60 μm region; before and after etching with KCN solution respectively. *Inset* optical image of a $CuInS_2$ film showing details area used for Raman micro-mapping analysis

is critical to the formation of the crystalline compound. The peaks are narrow and their relative intensity is similar to those in the diffraction cards of $CuInS_2$ (PDF 27-0159). The pattern displays an intense peak at 27.81° and weak peaks at 46.21° and 55.01°, which correspond to the (112), (204) or (220), and (116) or (312) reflections of the $CuInS_2$ phase, respectively. There is no evidence of formation of additional phases on the basis of XRD results.

Raman spectroscopy can be used as a complementary technique to XRD. Several authors have shown evidence indicating that the most intense Raman mode for the chalcopyrite (CH) structure is the A_1 mode at 290 cm^{-1} [12, 25–28]. An additional mode that can be seen at 305 cm^{-1} belongs to the Cu–Au ordering (CA) [12, 25]. The other peaks at 240 cm^{-1} $\left(E^3_{TO},\ B^2_{2\ TO}\right)$ and 340 cm^{-1} $\left(E^1_{LO}\right)$ represent Raman modes for CH ordering [12, 26]. Figure 3a shows average Raman spectra typical of annealed $CuInS_2$ films, before and after etching in KCN. It may be observed that there are five prominent peaks at 240, 290, 305, 320 and 470 cm^{-1}. The strong peaks at 290 and 305 cm^{-1} correspond to the A_1 mode for the CH structure and for the CA ordering, respectively [12, 25]. This is an indication that the film is a mixture of CH and CA orders. The broad peak that appears at 320 cm^{-1} may be assigned to β–In_2S_3 formed as secondary phase [28, 29]. The peak at 470 cm^{-1} can be attributed to $Cu_{2-x}S$. Before etching, a peak of $Cu_{2-x}S$ can be observed. After etching, the disappearance of the signal from this phase is evident and the presence of chalcopyrite phase is observed. These results are in good agreement with previously published work reporting the deposition of chalcogenide thin films on FTO and glass substrates [29].

The homogeneity, the spatial distribution of the chalcopyrite and secondary phases as well as the effect of etching were studied by Raman micro-maps as presented in Fig. 3b and c. The distribution of the CIS phase along the

Author's personal copy

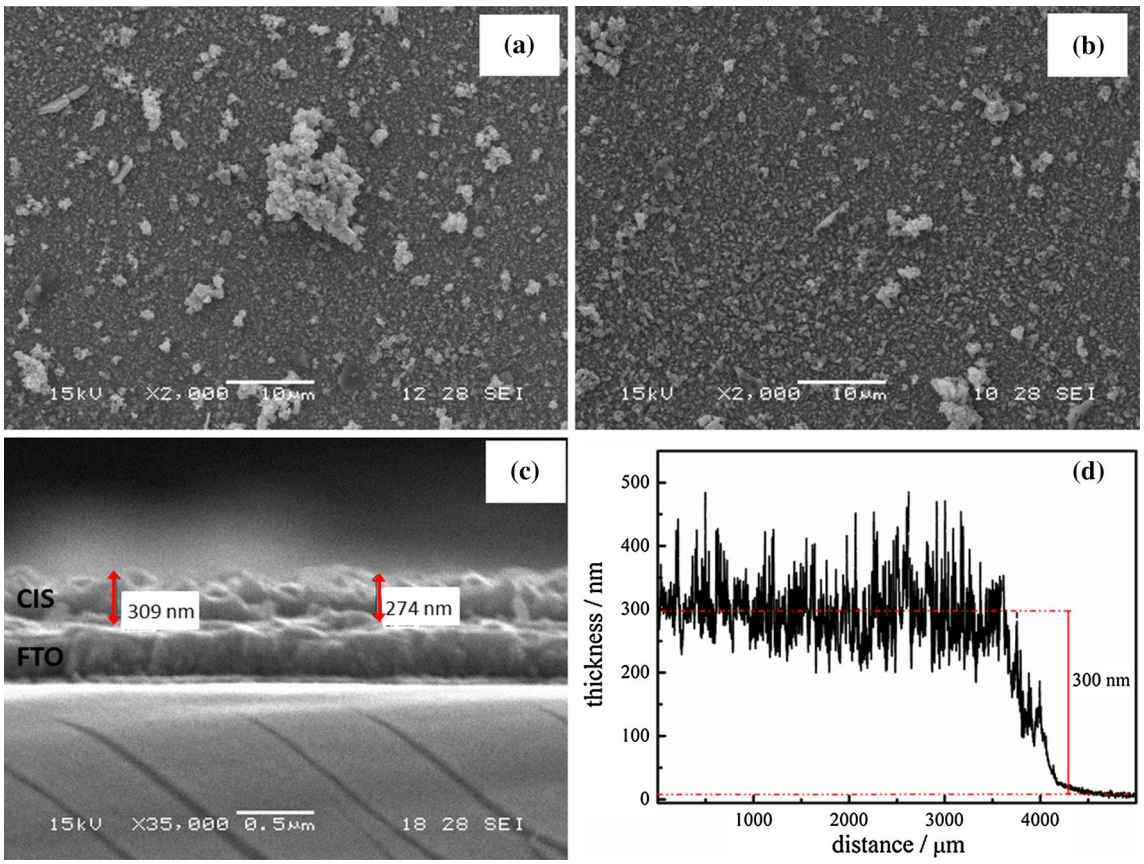

Fig. 4 SEM images of CIS films annealed in sulfur atmosphere at 450 °C for 90 min before **a** and after **b** etching with 0.5 mol L^{-1} of KCN solution during 30 s. **c** Cross sectional view of an annealed and etched film. **d** Profilometric scan of the CIS film, the average thickness is ~300 nm

film is homogeneous even in the annealed samples without etching along the whole area under analysis, as indicated by the signals at 290 and 305 cm^{-1}. This is even clearer after the etching.

3.2.2 *Surface morphology and elementary composition*

SEM images of the $CuInS_2$ film were taken to evaluate the effect of etching on the morphology of the surface. Figure 4 shows surface structures of the film before (Fig. 4a) and after etching (Fig. 4b). The degree of coverage is complete and homogeneous. The surface morphology shows agglomerates prior to etching. These can be attributed to $Cu_{2-x}S$ compounds which dissolve after etching in KCN. In this case, a more homogeneous film is formed, after partial removal of the binary compounds.

Figure 4c shows a cross-section view of an annealed and etched film deposited on FTO. This image illustrates average thickness values for the film (~300 nm). The average thickness was also evaluated using a profilometer (Fig. 4d). The resulting value is in agreement with the cross-section obtained with SEM (~300 nm).

Table 1 EDS results corresponding to the analysis of the films shown in Fig. 4

	% At Cu	% At In	% At S	Cu/S	In/S	Cu/In	S/Cu + In
Stoichiometric ratio	25	25	50	0.5	0.5	1	1
Before etching	30.4	16	53.6	0.57	0.3	1.9	1.15
After etching	25.1	20.6	54.3	0.46	0.4	1.2	1.2

According to the EDS results of the annealed samples (Table 1) before etching, the atomic ratios of Cu, In and S do not correspond to the stoichiometric ratio of CIS, due to the prevalence of binary compounds in the surface. After etching, the atomic ratio of the thin film shown in Fig. 4b is closer to the stoichiometric proportion of $CuInS_2$, in particular the Cu/In ratio. This is in agreement with the removal of the undesired phases already detected by micro Raman spectroscopy.

Figure 5a displays the XPS survey spectra of annealed thin films prior to the chemical attack with KCN. The binding energies obtained from the XPS analysis were

Author's personal copy

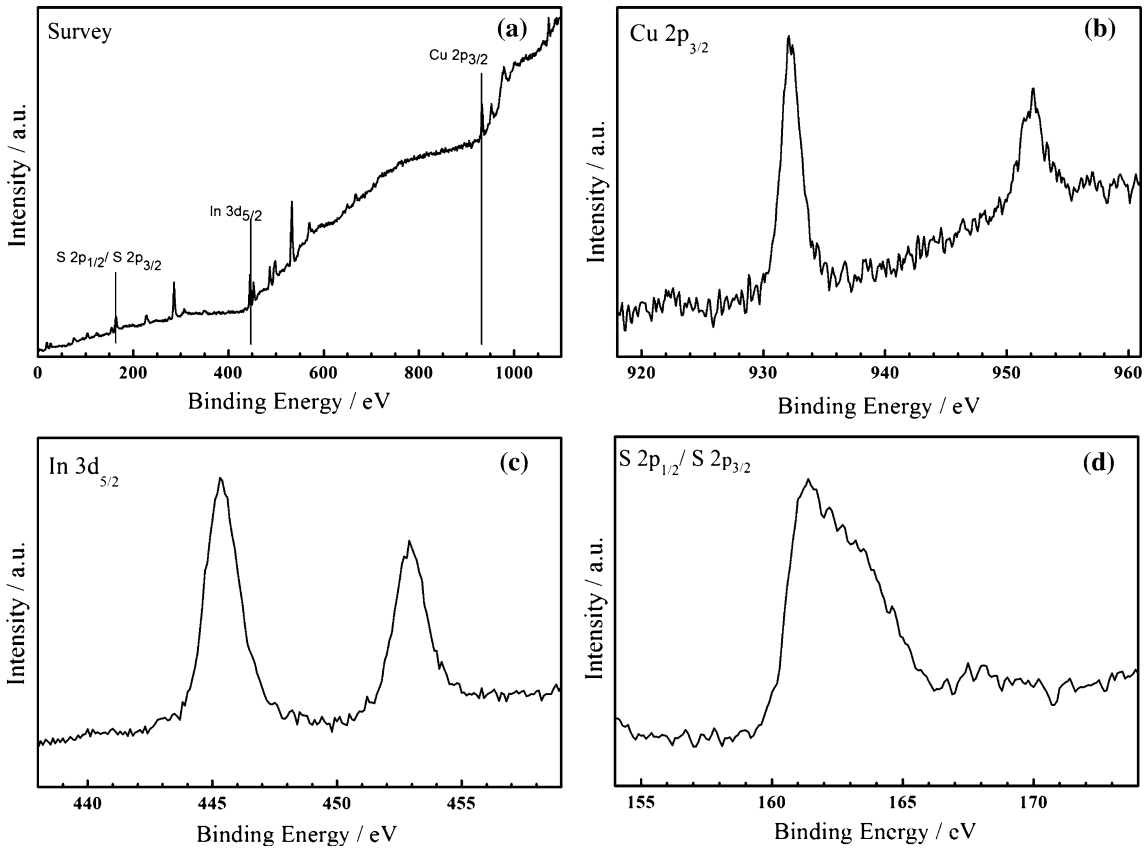

Fig. 5 **a** XPS survey spectrum of annealed $CuInS_2$ thin film prior to the chemical attack with KCN. **b** Cu 2p; **c** In 3d and **d** S 2p core-level spectra

corrected for C 1 s to 284.5 eV as reference. Figure 5b represents the Cu 2p core level spectrum. The observed peak located at 931.6 eV coincides with the binding energy for Cu $2p_{3/2}$ electrons emitted from $CuInS_2$ compound and the peak at 951 eV corresponds to the binding energy for Cu $2p_{1/2}$ electrons emitted from Cu element [24, 30]. It is worth noting that the satellite peak corresponding to the binding energy of Cu^{2+} usually located at 942 eV is not observed in the present XPS spectrum [31]. The observed binding energy peaks located at 445.3 and 452.8 eV (Fig. 5c) are attributed to the electronic states of In $3d_{5/2}$ and In $3d_{3/2}$. The value for S 2p binding energy (Fig. 5d) located at 161.5 eV is characteristic of sulfides [3, 24, 32, 33].

In summary, the binding energies found for these films are in good agreement to those of copper, indium and sulfur in $CuInS_2$ films [24, 34].

3.2.3 *Semiconducting properties: band gap energy and conduction type*

The transmission spectrum of an annealed $CuInS_2$ thin film after etching with KCN was recorded at room temperature (Fig. 6a). In order to achieve a correct determination of the optical bandgap, the zero absorption line should be properly selected. Reflections, dispersions and amorphous phases are taken into consideration and extracted from the experimental data [35]. Transmission spectra were used to estimate the corrected optical absorption coefficient α ($\alpha = \alpha_{exp} - \alpha_{back}$). Figure 6b shows the variation of $(\alpha h\nu)^2$ as a function of photon energy ($h\nu$) corresponding to an average from several measurements. The calculated band gap, Eg, results equal to 1.43 eV. Similar values have been reported in literature by several authors [1, 3, 12–15, 36].

The predominant type of conduction can be either *n*- or *p*-type depending on preparation methods and composition. In addition, the non-stoichiometry and the presence of intrinsic defects and secondary phases can be determining the conductivity type [1, 9, 13, 15, 37, 38]. Photoelectrochemistry can be used to elucidate the nature of the carriers. Figure 7 shows the photopotential and the photocurrent registered at open circuit potential for the films annealed and after chemical etching. With illumination, the potential moves to more positive values (positive photopotential) and the current moves in the negative

Author's personal copy

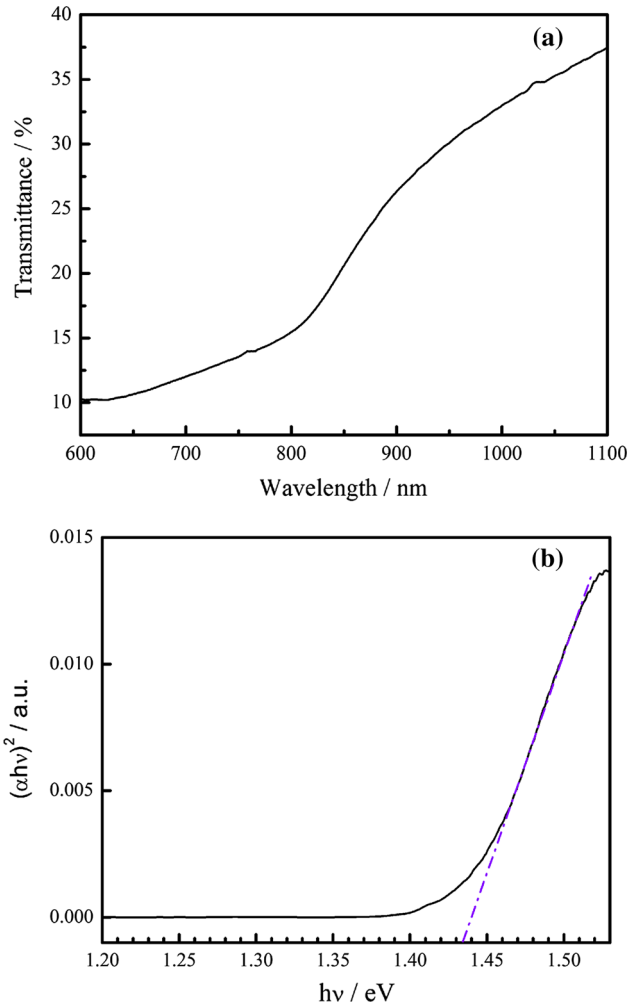

Fig. 6 **a** Optical transmittance spectrum of annealed thin films after etching with KCN at room temperature. **b** Plot of $(\alpha h\nu)^2$ versus $h\nu$ derived from the transmittance spectrum for electrodeposited CIS film on FTO substrate $E_g = 1.43$ eV

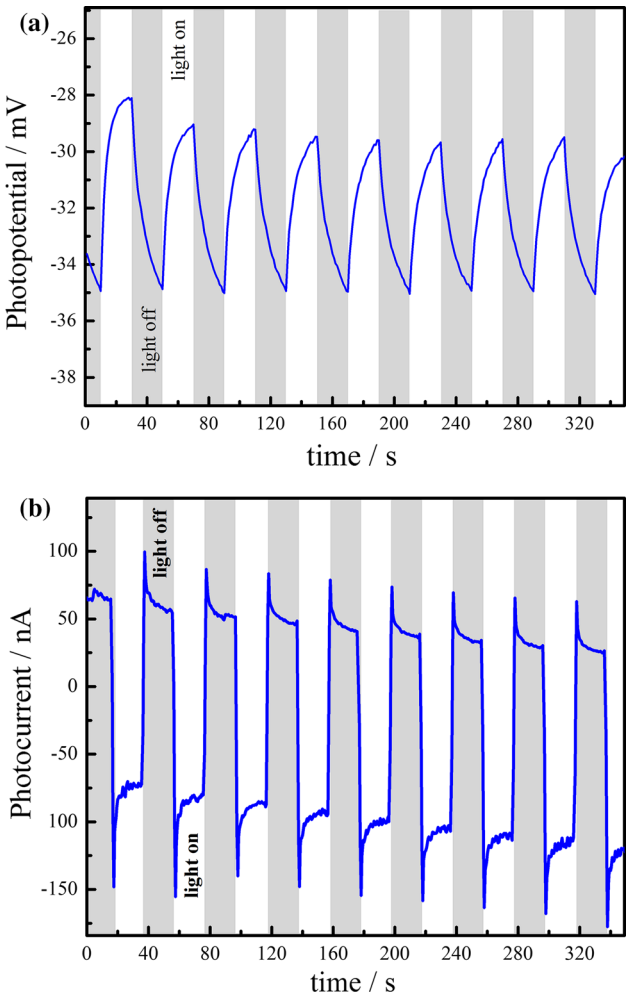

Fig. 7 **a** Photopotential and **b** photocurrent as function of time of CIS film after annealing in sulfur atmosphere and etching with 0.5 mol L^{-1} of KCN solution during 30 s. The measurements were performed using chopped light (20 s on/20 s off) in a solution of 0.1 mol L^{-1} KCl

direction (negative photocurrent), confirming the *p*-type nature of the film. A deeper explanation on the mechanism of electron transport to validate *p*-type nature and the photoresponse can be seen in our previous work [29].

4 Conclusions

$CuInS_2$ thin films were grown from a single bath at pH 8 by one-step electrodeposition on FTO substrate. After sulfurization crystalline CIS was clearly identified as the main component of the deposited film. Etching in KCN solution guarantees the removal of secondary phases that are detrimental for the electronic properties of the deposit. According to the XRD patterns, XPS and Raman spectra, the predominant phase corresponds to $CuInS_2$ chalcopyrite.

Photoelectrochemical tests confirm *p*-type conduction. The band gap energy was estimated from absorption spectra, resulting in a value in good agreement with results published for CIS prepared by other methods.

The results are in good agreement with those from previous investigations carried out using acidic precursors. The electrolyte used in this work can be recommended for the substrates with poor resistance to acidic etching, providing a versatile method for the electrodeposition of $CuInS_2$ on various substrates.

Acknowledgments The authors acknowledge the financial support received from the Consejo Nacional de Investigaciones Científicas y Técnicas (CONICET), Agencia Nacional de Promoción Científica y Tecnológica (ANPCyT, PICT 2634), and Universidad Nacional de Mar del Plata (UNMdP). We are also grateful to PhD Mariela Desimone for her assistance with XRD and Raman measurements and Eng. Sheila Omar for her assistance with the profilometer.

Author's personal copy

References

1. Cheng K-W, Chiang W-H (2011) Effect of [Cu]/[Cu + In] ratio in the solution bath on the growth and physical properties of $CuInS_2$ film using one-step electrodeposition. J Electroanal Chem 661(1):57–65. doi:10.1016/j.jelechem.2011.07.013
2. Valdés MH, Berruet M, Goossens A, Vázquez M (2010) Spray deposition of $CuInS_2$ on electrodeposited ZnO for low-cost solar cells. Surf Coat Tech 204(24):3995–4000. doi:10.1016/j.surfcoat.2010.05.028
3. Xu XH, Wang F, Liu JJ, Park KC, Fujishige M (2011) A novel one-step electrodeposition to prepare single-phase $CuInS_2$ thin films for solar cells. Sol Energy Mater Sol Cells 95(2):791–796. doi:10.1016/j.solmat.2010.10.025
4. Liu R, Liu Y, Liu C, Luo S, Teng Y, Yang L, Yang R, Cai Q (2011) Enhanced photoelectrocatalytic degradation of 2,4-dichlorophenoxyacetic acid by $CuInS_2$ nanoparticles deposition onto TiO_2 nanotube arrays. J Alloy Compd 509(5):2434–2440. doi:10.1016/j.jallcom.2010.11.040
5. Goossens A, Hofhuis J (2008) Spray-deposited $CuInS_2$ solar cells. Nanotechnology. doi:10.1088/0957-4484/19/42/424018
6. Terasako T, Uno Y, Inoue S, Kariya T, Shirakata S (2006) Structural, optical and electrical properties of $CuInS_2$ thin films prepared by chemical spray pyrolysis. Phys Status Solidi (c) 3(8):2588–2591. doi:10.1002/pssc.200669597
7. Amara A, Rezaiki W, Ferdi A, Hendaoui A, Drici A, Guerioune M, Bernède JC, Morsli M (2007) Electrical and optical characterisation of $CuInS_2$ crystals and polycrystalline coevaporated thin films. Sol Energy Mater Sol Cells 91(20):1916–1921. doi:10.1016/j.solmat.2007.07.007
8. Chang C-C, Liang C-J, Cheng K-W (2009) Physical properties and photoresponse of Cu–Ag–In–S semiconductor electrodes created using chemical bath deposition. Sol Energy Mater Sol Cells 93(8):1427–1434. doi:10.1016/j.solmat.2009.03.014
9. Yukawa T, Kuwabara K, Koumoto K (1996) Electrodeposition of $CuInS_2$ from aqueous solution (II) electrodeposition of $CuInS_2$ film. Thin Solid Films 286(1–2):151–153. doi:10.1016/S0040-6090(96)08545-8
10. Nakamura S, Yamamoto A (1997) Preparation of $CuInS_2$ films with sufficient sulfur content and excellent morphology by one-step electrodeposition. Sol Energy Mater Sol Cells 49(14):415–421. doi:10.1016/S0927-0248(97)00122-0
11. Nakamura S, Yamamoto A (2003) Electrodeposited $CuInS_2$ based thin film solar cells. Sol Energy Mater Sol Cells 75(1–2):81–86. doi:10.1016/S0927-0248(02)00097-1
12. Sanchez S, Aldakov D, Rouchon D, Rapenne L, Delamoreanu A, Lévy-Clémentm C, Ivanova V (2013) Sensitization of ZnO nanowire arrays with $CuInS_2$ for extremely thin absorber solar cells. J Renew Sust Energy. doi:10.1063/1.4791780
13. Yuan J, Shao C, Zheng L, Fan M, Lu H, Hao C, Tao D (2014) Fabrication of $CuInS_2$ thin film by electrodeposition of Cu–In alloy. Vacuum 99:196–203. doi:10.1016/j.vacuum.2013.06.005
14. Lu L, Wang Y, Li X (2012) Influence of processing parameters on the preparation of $CuInS_2$ thin film by one-step electrodeposition as the solar cell absorber. Surf. Coat. Tech. 212:55–60. doi:10.1016/j.surfcoat.2012.03.097
15. Martinez AM, Fernández AM, Arriaga LG, Cano U (2006) Preparation and characterization of Cu–In–S thin films by electrodeposition. Mater Chem Phys 95(2–3):270–274. doi:10.1016/j.matchemphys.2005.06.018
16. Asenjo B, Chaparro AM, Gutiérrez MT, Herrero J (2006) Electrochemical growth and properties of $CuInS_2$ thin films for solar energy conversion. Thin Solid Films 511–512:117–120. doi:10.1016/j.tsf.2005.11.092
17. Berruet M, Vázquez M (2010) Electrodeposition of single and duplex layers of ZnO with different morphologies and electrical properties. Mater Sci Semicon Proc 13(4):239–244. doi:10.1016/j.mssp.2010.08.001
18. Kärber E, Abass A, Khelifi S, Burgelman M, Katerski A, Krunks M (2013) Electrical characterization of all-layers-sprayed solar cell based on ZnO nanorods and extremely thin CIS absorber. Sol Energy 91:48–58. doi:10.1016/j.solener.2013.01.020
19. Li Y, Liu Z, Wang Y, Liu Z, Han J, Ya J (2012) ZnO/$CuInS_2$ core/shell heterojunction nanoarray for photoelectrochemical water splitting. Int J Hydrogen Energy 37(20):15029–15037. doi:10.1016/j.ijhydene.2012.07.117
20. Berruet M, Valdés M, Ceré S, Vázquez M (2012) Cost-effective solar cells containing copper indium chalcogenides prepared by SILAR method. J Mater Sci 47(5):2454–2460. doi:10.1007/s10853-011-6067-6
21. Bär M, Klaer J, Weinhardt L, Wilks RG, Krause S, Blum M, Yang W, Heske C, Schock H-W (2013) $Cu_{2-x}S$ surface phases and their impact on the electronic structure of $CuInS_2$ thin films—a hidden parameter in solar cell optimization. Adv Energy Mater 3(6):777–781. doi:10.1002/aenm.201200946
22. Wilhelm T, Berenguier B, Aggour M, Kanis M, Lewerenz H-J (2006) Efficient $CuInS_2$ (CIS) solar cells by photoelectrochemical conditioning. C R Chim 9(2):294–300. doi:10.1016/j.crci.2005.02.047
23. He YB, Krämer T, Österreicher I, Polity A, Meyer BK, Hardt M (2005) Post-growth treatment effects on properties of $CuInS_2$ thin films deposited by RF reactive sputtering. Semicond Sci Tech 20(8):685. doi:10.1088/0268-1242/20/8/006
24. Wagner WMRCD, Davis LE, Moulder JF, Muilengerg GE (1978) Handbook of X-ray photoelectron spectroscopy. Perkin-Elmer Corporation, Minnesota
25. Álvarez-García J, Marcos-Ruzafa J, Pérez-Rodríguez A, Romano-Rodríguez A, Morante JR, Scheer R (2000) MicroRaman scattering from polycrystalline $CuInS_2$ films: structural analysis. Thin Solid Films 361:208–212. doi:10.1016/S0040-6090(99)00847-0
26. Rudigier E, Alvarez-Garcia J, Luck I, Klaer J, Scheer R (2003) Quality assessment of chalcopyrite thin films using Raman spectroscopy. J Phys Chem Solids 64(9–10):1977–1981. doi:10.1016/S0022-3697(03)00154-9
27. Oja I, Nanu M, Katerski A, Krunks M, Mere A, Raudoja J, Goossens A (2005) Crystal quality studies of $CuInS_2$ films prepared by spray pyrolysis. Thin Solid Films 480–481:82–86. doi:10.1016/j.tsf.2004.11.013
28. Lee DY, Kim J (2010) Characterization of sprayed $CuInS_2$ films by XRD and Raman spectroscopy measurements. Thin Solid Films 518(22):6537–6541. doi:10.1016/j.tsf.2010.03.062
29. Berruet M, Schreiner WH, Ceré S, Vázquez M (2011) Deposition and characterization of $CuInSe_2$ films for solar cells using an optimized chemical route. J Alloy Compd 509(6):3019–3024. doi:10.1016/j.jallcom.2010.11.190
30. Kim CR, Han SY, Chang CH, Lee TJ, Ryu SO (2010) Synthesis and characterization of $CuInSe_2$ thin films for photovoltaic cells by a solution-based deposition method. Curr Appl Phys 10(3, Supplement): S383–S386. doi: 10.1016/j.cap.2010.01.006
31. Chen H, Yu SM, Shin DW, Yoo JB (2010) Solvothermal Synthesis and Characterization of Chalcopyrite $CuInSe_2$ Nanoparticles. Nanoscale Res Lett 5(1):217–223. doi:10.1007/s11671-009-9468-6
32. Calderón C, Oyola JS, Bartolo-Pérez P, Gordillo G (2013) Studies in $CuInS_2$ based solar cells, including ZnS and In_2S_3 buffer layers. Mater Sci Semicon Proc 16(6):1382–1387. doi:10.1016/j.mssp.2013.06.011

Author's personal copy

33. Katerski A, Mere A, Kazlauskiene V, Miskinis J, Saar A, Matisen L, Kikas A, Krunks M (2008) Surface analysis of spray deposited copper indium disulfide films. Thin Solid Films 516(20):7110–7115. doi:10.1016/j.tsf.2007.12.027
34. Han S, Kong M, Guo Y, Wang M (2009) Synthesis of copper indium sulfide nanoparticles by solvothermal method. Mater Lett 63(13–14):1192–1194. doi:10.1016/j.matlet.2009.02.032
35. Berruet M, Pereyra CJ, Mhlongo GH, Dhlamini MS, Hillie KT, Vázquez M, Marotti RE (2013) Optical and structural properties of nanostructured ZnO thin films deposited onto FTO/glass substrate by a solution-based technique. Opt Mater 35(12):2721–2727. doi:10.1016/j.optmat.2013.08.018
36. Cayzac R, Boulc'h F, Bendahan M, Pasquinelli M, Knauth P (2008) Preparation and optical absorption of electrodeposited or sputtered, dense or porous nanocrystalline $CuInS_2$ thin films. C R Chim 11(9):1016–1022. doi:10.1016/j.crci.2008.02.003
37. Bandyopadhyaya S, Chaudhuri S, Pal AK (2000) Synthesis of $CuInS_2$ films by sulphurization of Cu/In stacked elemental layers. Sol Energy Mater Sol Cells 60(4):323–339. doi:10.1016/S0927-0248(99)00064-1
38. Xu X, Wang F, Liu J, Ji J (2010) Effect of potassium hydrogen phthalate ($C_8H_5KO_4$) on the one-step electrodeposition of single-phase $CuInS_2$ thin films from acidic solution. Electrochim Acta 55(15):4428–4435. doi:10.1016/j.electacta.2010.02.077